17th World Conference on Earthquake Engineering, 17WCEE
Sendai, Japan - September 13th to 18th 2020

INFLUENCE OF PREVIOUS SEISMIC DEGRADATION OF R.C. BUILDINGS IN THE CASE OF RETROFITTING BY DAMPED BRACES

F. Mazza[1], C. Pasceri[2]

[1] *Professor, Department of Civil Engineering, University of Calabria, fabio.mazza@unical.it*
[2] *Research fellow, Department of Civil Engineering, University of Calabria, carlopasceri@gmail.com*

Abstract

Supplementary energy dissipation is an efficient technique for the seismic retrofitting of a reinforced concrete (r.c.) framed building as long as structural behaviour before failure and sensitivity to damage is evaluated properly. In fact, lack of knowledge on strength and stiffness degradation may not be compensated for in the calculation of a passive control system. On the other hand, the widespread use of supplementary energy dissipation devices is closely related to the availability of simplified yet reliable design procedures along with the new generation of seismic codes based on performance-based design. These observations open up the way for a more realistic estimation of the deformation capacity through a displacement based design procedure in which previous seismic degradation of the multi-degree-of-freedom (MDOF) model of the actual structure is evaluated starting from the initial backbone curve of the corresponding single-degree-of-freedom (SDOF) system. Specifically, the nonlinear static analysis of the MDOF system can generate an idealized force-displacement curve of the equivalent SDOF system, so that an estimation of the seismic capacity of the original structure in terms of the capacity boundary curve is obtained by nonlinear dynamic analysis of the equivalent SDOF system. To evaluate the effectiveness of the proposed design procedure of hysteretic damped braces (HYDBs), the RINTC project, financed by the Italian Department of Civil Protection, has selected an archetype as representative of the Italian residential housing stock constructed during the 1990s. A simulated design of a six-storey reinforced concrete (r.c.) building with rectangular shape, five and three bays along the principal in-plan directions, is carried out in line with the Italian code for a moderate seismic zone. Three configurations of masonry infills (MIs) are considered: Bare Frame (BF, with nonstructural MIs); Infilled Frame (IF, with an uniform in-elevation distribution of structural MIs); Pilotis Frame (PF, with no MIs at the ground floor and structural MIs at the other floors). OpenSees is the computational platform for nonlinear seismic analysis. A lumped plasticity model is adopted for r.c. frame members, with moment-chord rotation at critical end sections defined by the modified peak-oriented Ibarra-Medina-Krawinkler deterioration model, also accounting for shear failure mode. The shear behaviour of the beam-column joints is modelled by means of rigid offsets, reflecting the joint panel dimensions, and a zero-length rotational spring defined through a quadri-linear moment-rotation relationship. A simplified diagonal pin-jointed strut model takes into account the in-plane failure modes that can occur in the infill panels when subjected to seismic loading (i.e. diagonal compression, crushing the corners in contact with the frame, sliding shear along horizontal joints and diagonal tension), while a bilinear model describes the nonlinear response of the HYDBs. Finally, nonlinear bi-directional dynamic analyses of the unbraced and damped braced BF, IF and PF structures are carried out, with or without seismic damage, with reference to records scaled in line with the hypotheses adopted.

Keywords: r.c. framed structures; strength and stiffness degradation; hysteretic damped braces; displacement-based design procedure; seismic retrofitting.

1. Introduction

The effectiveness of the seismic retrofitting of an as-built building is strictly related to the correct assessment of the level of damage expected after an earthquake, because lack of knowledge on strength and stiffness degradation may not be compensated for in the calculation. Moreover, cyclic degradation of strength and stiffness, at a given deformation level under reverse cyclic loading, and in-cycle degradation, under increasing deformations within one loading excursion of a cycle, should be distinguished because they do not contribute to damage levels to the same extent [1]. These considerations highlight that complex nonlinear models are essential to reproduce all deterioration modes in the hysteretic behaviour under large seismic loads. On the other hand, the widespread use of passive control systems based on damped braces (i.e. energy dissipation devices inserted on steel braces) is strictly related to the availability of simplified yet reliable performance-based design procedures [2]. Within this context, pushover analysis is generally viewed as a reliable tool for evaluating the extent of damage experienced at a target displacement. In particular, the Displacement-Based-Design (DBD) approaches assign a target deformation corresponding to a performance objective (e.g. they avoid structural collapse and/or reduce non-structural damage), combining the nonlinear static analysis of the multi-degree-of-freedom (MDOF) model of the structure with the response spectrum analysis of an equivalent single-degree-of-freedom (SDOF) system [3, 4]. However, cyclic effect of the seismic loading is not modelled in nonlinear static analysis so that the initial backbone (i.e. the monotonic loading curve) and the cyclic envelope (i.e. the curve enveloping the hysteretic response) laws are usually different, as the latter may be heavily loading-history dependent [5].

The aim of the present work is to evaluate the influence of previous seismic degradation of reinforced concrete (r.c.) framed buildings on retrofitting by means of hysteretic damped braces (HYDBs). A simulated design of a six-storey archetype in L'Aquila, representative of the Italian residential housing stock during the 1990s, is made assuming the second seismic category required at the time of construction [6]. First, nonlinear static analysis of the MDOF model of the building is carried out with the OpenSees code [7], assuming three in-elevation configurations of masonry infills (MIs) uniformly distributed in plan along the perimeter: i) Bare Frame (BF), with nonstructural MIs; ii) Infilled Frame (IF), with an uniform in-elevation distribution of structural MIs; iii) Pilotis Frame (PF), with no MIs at the ground level and structural MIs at the other floors. A lumped plasticity model is adopted for r.c. frame members, with flexure- or shear-controlled (prior to or following flexural yielding) moment-chord rotation at critical end sections [8]. The shear behaviour of the beam-column joints is modelled by means of rigid offsets and a scissor model [9]. Structural MIs are modelled with a simplified diagonal pin-jointed strut model taking into account the in-plane failure modes and the presence of openings [10]. Then, a DBD procedure of the HYDBs is applied to attain a designated performance level for a specific level of seismic intensity and a given level of damage [3, 11]. A hysteretic model based on plastic and damage mechanisms is adopted to represent the degrading response of r.c. frame members [5]. Specifically, cyclic behaviour is taken into account replacing the initial backbone curve of the SDOF system equivalent to the BF, IF and PF by a sequence of N linear segments defined by a combination of as many elastic-perfectly plastic (EPP) mechanisms as necessary. Cyclic deterioration is reproduced by introducing N elastic-softening damage (ESD) mechanisms acting in-parallel with the EPP ones, controlled by a damage index. The stiffness distribution of the HYDBs is designed to exclude soft storey behaviour for the PF structure, assuming the same value of the drift ratio at each storey, while a proportional stiffness criterion is applied for the BF and IF structures [4]. Finally, nonlinear dynamic analyses of the unbraced and damped braced structures with or without seismic damage are carried out, considering records scaled in line with the design hypotheses adopted.

2. Layout and design of the original archetype building

An archetype representative of the Italian residential housing stock constructed during the 1990s is selected from the RINTC project [6], financed by the Italian Department of Civil Protection. Specifically, an r.c. framed structure regular in-plan (Fig. 1a), with five and three bays along the principal X and Y directions,

and in-elevation (Fig. 1b), where double leaf (8 cm, internal layer, and 12 cm, external layer) masonry infills (MIs) of hollow clay bricks only contribute to the dead load, is assumed located in L'Aquila (Italy). Deep beams are placed in the perimeter frames and in the knee configuration of the staircase, with cross section 30cm×60cm at the first two levels and 30cm×50cm at the other four levels, while all internal beams are flat with a cross-section 60cm×25cm and 80cm×25cm (the latest marked with an asterisk in Fig 1a). Rectangular cross-section with the orientation shown in Fig. 1a is assumed for the columns, considering: 30cm×60cm at the first two levels; 30cm×50cm at the third and fourth levels; 30cm×40cm at the fifth and roof levels. The percentage of openings varies depending on the architectural layout is assumed for the MIs, marked with different colours in Figs. 1a,b: i.e. 0%, MI.B in brown; 40%, MI.O in orange; 22%, MI.Y in yellow.

A simulated design of the bare frame (BF) is carried out in line the technical codes DM92 [12] and DM86 [13] for the vertical and seismic loads, respectively, considering linear static analysis and the admissibile tension method. Vertical gravity loads are represented by dead loads of 4.8 kN/m^2, on the roof, and 6.3 kN/m^2, on the other floors, and live loads of 2.2 kN/m^2, on the roof (snow), 2 kN/m^2, on the other floors, and 4 kN/m^2 for the staircase. Non-structural MIs are taken into account through an additional dead load of 3.5 kN/m^2, along the perimeter, with compressive and shear strength equal to 2 MPa and 0.4 MPa, respectively. Horizontal seismic loads are evaluated for a medium-risk zone (seismic coefficient, C=0.07) and typical subsoil class (foundation coefficient, ε=1). Concrete with cylindrical compressive strength of 25 MPa (maximum normal stress equal to 8.5 MPa) and steel reinforcement with yield strength of 430 MPa (maximum normal stress equal to 2600 MPa) are considered. The longitudinal reinforcement ratio is included in the ranges 0.25%-0.67% and 0.40%-1.26% for deep and flat beams, respectively, while the range 0.75%-1.90% is assumed for the columns. The transversal reinforcement is made with 8 mm hoops with constant spacing in the ranges 13cm-19cm and 7cm-17cm for deep and flat beams, respectively, and 12cm-15cm, for columns. Minimum conditions provided by DM92 are also satisfied for the longitudinal and transversal bars of the r.c. frame members. Further details can be found in [6].

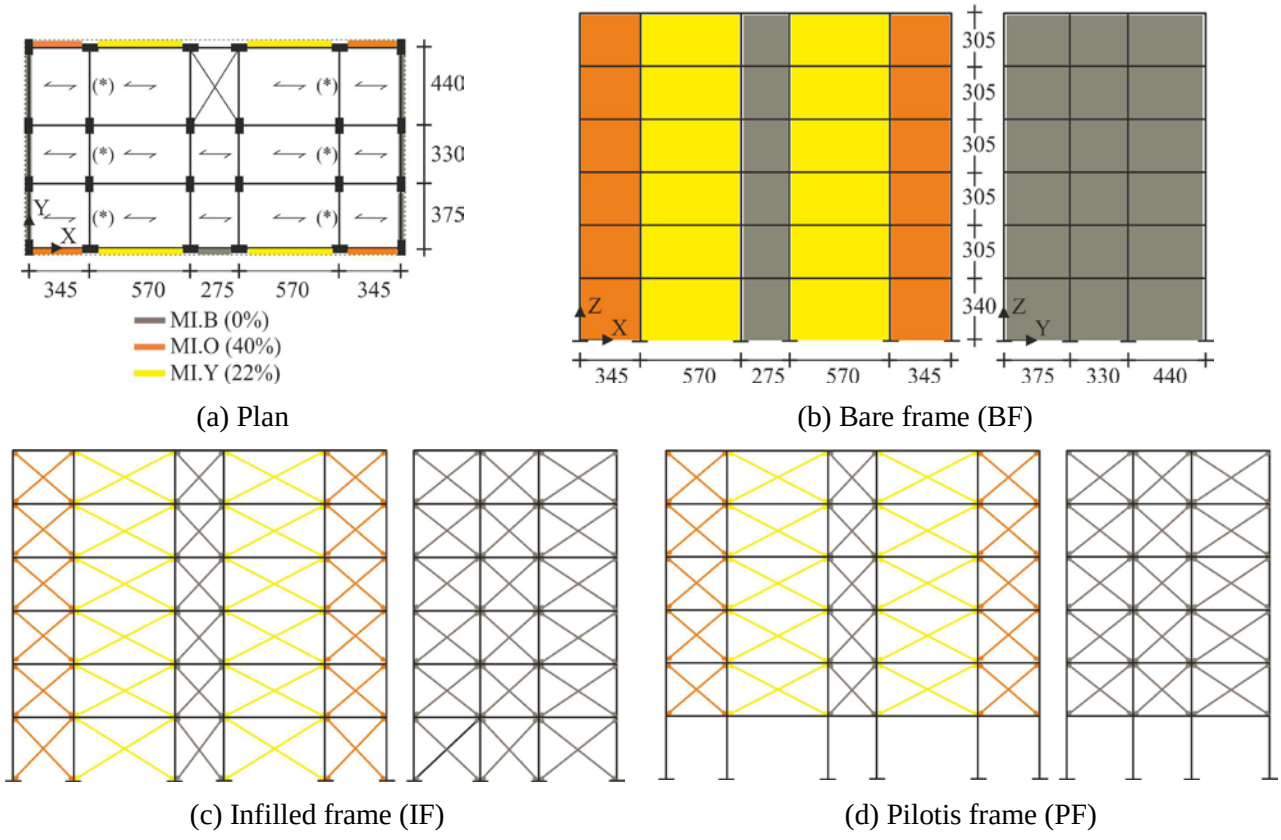

(a) Plan (b) Bare frame (BF)

(c) Infilled frame (IF) (d) Pilotis frame (PF)

Fig. 1 – Alternative layouts of the original test structure (unit in cm)

Three configurations of MIs are considered for the original test structure: i.e. bare frame (BF), with nonstructural MIs designed so as not to affect structural deformability (Fig. 1b); ii) infilled frame (IF), with structural MIs uniformly distributed along the height, in contact with the frame but not structurally connected to it (Fig. 1c); pilotis frame (PF), with a soft-storey at the ground level and the same MIs of the IF at the other levels. Dynamic properties of the four main vibration modes for the BF, IF and PF structures, two for each in-plan principal direction, are reported in Table 1 together with the total mass of the building (m_{tot}): i.e. vibration periods (T_{iX} and T_{iY}, i=1,2) and translational effective mass (m_{iX} and m_{iY}, i=1,2), expressed as a percentage of m_{tot}.

Table 1 – Dynamic properties of the test structures (units in t, m and s)

Structure	$\mathbf{m_{tot}}$	$\mathbf{T_{1X}}$	$\mathbf{m_{1X}\,[\%m_{tot}]}$	$\mathbf{T_{1Y}}$	$\mathbf{m_{1Y}\,[\%m_{tot}]}$	$\mathbf{T_{2X}}$	$\mathbf{m_{2X}\,[\%m_{tot}]}$	$\mathbf{T_{2Y}}$	$\mathbf{m_{2Y}\,[\%m_{tot}]}$
BF	1566	1.302	79	0.961	77	0.455	13	0.329	8
IF	1566	0.618	84	0.587	84	0.211	11	0.201	11
PF	1566	0.766	93	0.651	89	0.245	5	0.219	9

Nonlinear static analysis of the original test structures is carried out with reference to invariant lateral force distributions, applied at the centre of mass of each floor level along the in-plan X and Y directions, increasing proportionally to the floor masses with ("modal type") or without ("uniform type") considering the fundamental vibration mode. Pushover analyses are terminated once one of the following mechanisms is attained for strucural and nonstructural elements [7]. Specifically, a lumped plasticity model is adopted for r.c. frame members, with a backbone (trilinear) moment-chord rotation at critical end sections (characterized by elastic, hardening and post-capping stiffnesses) defined by the modified peak-oriented Ibarra-Medina-Krawinkler deterioration model [8]. Bilinear and trilinear (reduced) moment-chord rotation laws are assumed for the shear-critical elements accounting for shear failure modes prior to or following the flexural yielding, respectively. The shear behaviour of the beam-column joints is modelled by means of rigid offsets, reflecting the joint panel dimensions, and a zero-length rotational spring which is described by four points representing [9]: initial concrete joint cracking; beam reinforcement yielding or significant opening of existing cracks; peak loading; residual joint shear and rotation when damage to the joint is severe. Two types of failure are considered, depending on the shear demand of the joint: shear failure prior to beam reinforcement yielding (i.e. J-type failure); shear failure with beam reinforcement yielding (i.e. BJ-type failure). Finally, an equivalent single strut (concentric) model is adopted for MIs, with a trilinear backbone lateral force-storey drift curve consisting of the uncracked, post cracking and post-peak strength deterioration branches up to a conventional collapse point. The maximum lateral strength of the strut is evaluated with respect to four in-plane failure modes [10]: equivalent compressive strengths for diagonal compression; crushing in the corners in contact with the frame; sliding shear along horizontal joints and diagonal tension.

To complete the above, capacity curves representing normalized base shear (i.e. V_{base}/W_{tot},W_{tot} being the total seismic weight) and horizontal top displacement (i.e. d_{top}/H_{tot}, H_{tot} being the total height) of the BF, IF and PF original structures, along the longitudinal (X) and transversal (Y) planes, are plotted in Figs. 2a, 2b and 2c, respectively. Specifically, eight curves are plotted for each structure, referring to the positive and negative loading directions and for both loading patterns mentioned above. From comparison of the capacity curves, all parameters being equal for each structure, it emerges that maximum strength is always obtained in the Y direction, depending on the in-plan orientation of the cross-sections of all interior columns and most of the exterior ones (see Fig. 1a). Moreover, the lowest capacity curve is the one that corresponds to the modal load pattern. Analysis of bare and infilled frames has confirmed that the presence of MIs results in increased shear strength (Figs. 2b and 2c), which is more evident in the Y direction where perimeter MIs without openings are placed (see Fig. 1a). Attention will be given below to the modal capacity curves characterized by the lowest shear strength at the performance displacement $d_p=0.5\%/H_{tot}$, selected as design value of the HYDBs against the structural collapse and infill damage.

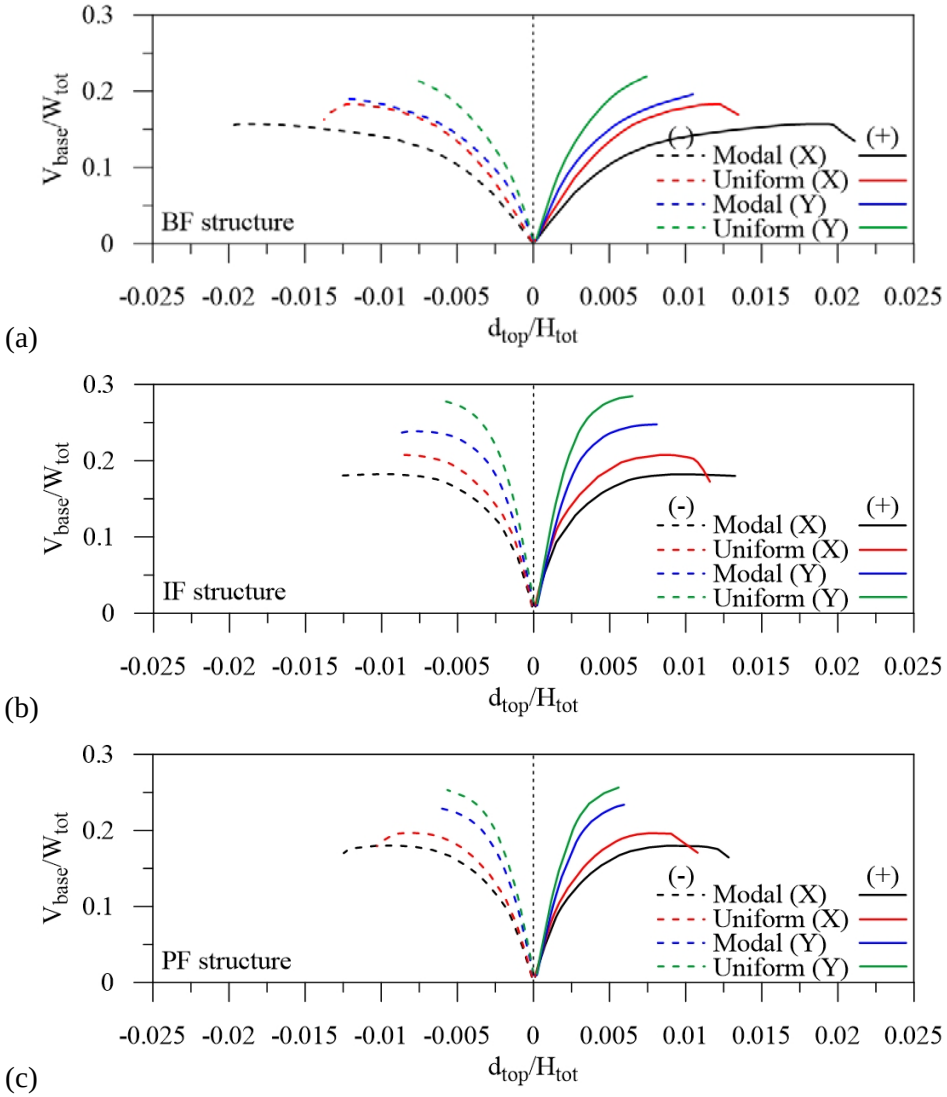

Fig. 2 – Comparison of pushover curves for the alternative layouts of the original test structure

2. Layout and retrofitting of the original archetype building

The seismic retrofitting of the archetype building is carried out by the insertion of diagonal steel braces equipped with hysteretic dampers (HYDBs); attention is taken to avoid impeding the internal functioning of the building and only the corner bays of the perimeter frames are involved to ensure compatibility with the architectural layout providing the lowest percentage (X direction) and absence (Y direction) of balcony doors (Fig. 3a). The influence of the stiffness of the supporting brace is not considered (i.e. brace stiffness $K_B \rightarrow \infty$), so that lateral stiffness of the HYDB (K_{DB}) and HYD (K_D) is assumed equal; this is also for the corresponding stiffness hardening ratios (i.e. $r_{DB}=r_D=3\%$). Three alternative retrofits are designed, with reference to the bare (i.e. Damped Braced Bare Frame, DBBF in Fig. 3b), infilled (Damped Braced Infilled Frame, DBIF in Fig. 3c) and pilotis (i.e. Damped Braced Pilotis Frame, DBPF in Fig. 3d) structures. Moreover, two distributions of the HYDBs are adopted along the height, according to: i) a proportional stiffness criterion, for the regular BF and IF original structures, assuming that mode shapes of the structures remain practically the same after the insertion of the HYDBs; ii) a constant drift criterion, for the original irregular PF structure, to obtain a globally regular retrofit by balancing the soft-storey at the ground level. Moreover, the vertical distribution of the yield load of the HYDBs is assumed proportional to the stiffness distribution.

The displacement design spectrum at the life-safety (LS) limit state is defined considering the current (DM18) provisions of the Italian code [14] for a residential building (functional class II, coefficient of use C_U=1.0 and expected life of 50 years) located in L'Aquila (13.40° longitude and 42.35° latitude). A high-risk seismic zone (i.e. peak ground acceleration on rock, a_g=0.261g) and moderately-soft subsoil (i.e. class C, site amplification factor S=1.33) are assumed. The computer code SeismoArtif [15] is used for the generation of a far-fault (inter-plate) artificial earthquake matching the LS design spectrum of acceleration provided by DM18, in the range of vibration periods 0.05s-4s containing the prescribed lower (T_{min}=0.15s) and upper ($T_{max}=2T_1$, where T_1 is the fundamental vibration period) bound limits.

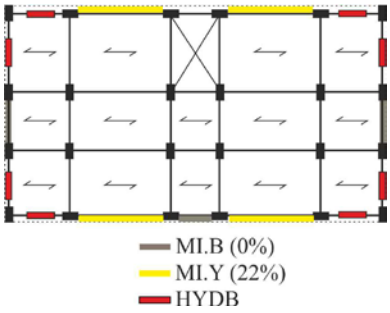

(a) Plan

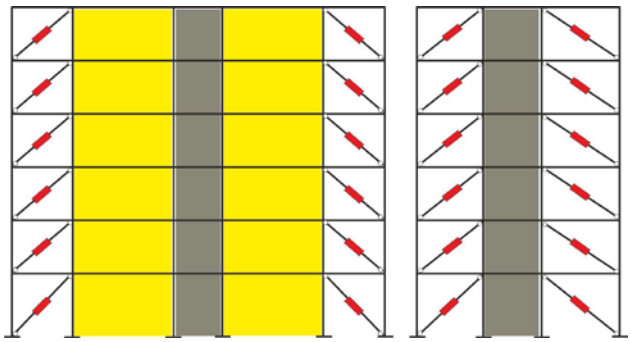

(b) Damped braced bare frame (DBBF)

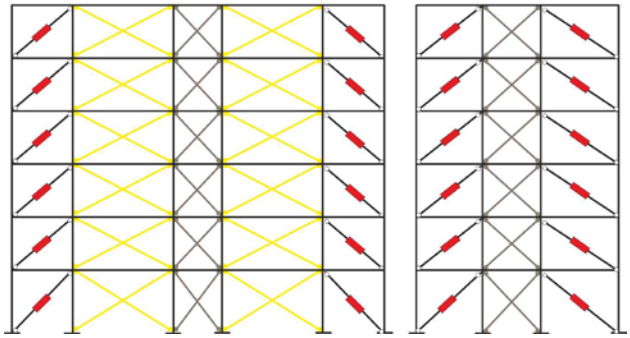

(c) Damped braced infilled frame (DBIF)

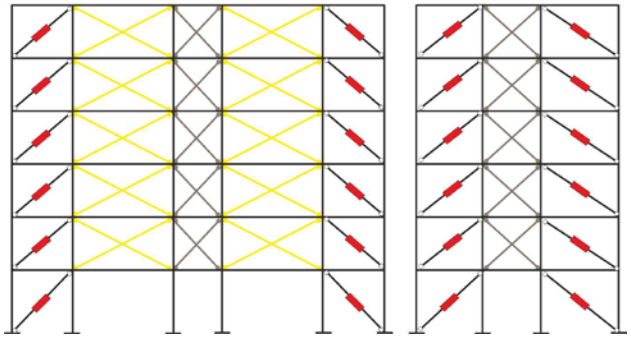

(d) Damped braced pilotis frame (DBPF)

Fig. 3 – Alternative layouts of the retrofitted test structure

A multistep iterative Displacement-Based-Design (DBD) procedure of HYDBs, previously proposed for in-elevation regular [3] and irregular [4] r.c. framed buildings, is applied for seismic retrofitting of the BF, IF and PF structures. In the following, attention is paid to the description of seismic damage of the SDOF system equivalent to the original MDOF structure [11], which results in modified values of the elastic stiffness ($K_{DB,e}$) and yield ($V_{yDB,e}$) and performance ($V_{pDB,e}$) loads of the equivalent damped brace when compared with values for the undamaged structure. First, the initial backbone curve of the SDOF system, is fitted by means of a trilinear function without (Fig. 4a) or with (Fig. 4b) softening. The hysteretic model obtained by the in-parallel combination of elastic-perfectly plastic (EPP) laws is adopted to account for the cyclic behaviour mechanisms, where the i-th linear segment of the piecewise linear fit is coupled with the corresponding i-th plastic mechanism described by the following expressions

$$V^{*\pm}_{P,i}=K^{\pm}_{P,i}\cdot\left(d^{*\pm}-d^{*\pm}_{y,i-1}\right),\ \left|d^{*\pm}_{y,i-1}\right|<\left|d^{*\pm}\right|\le\left|d^{*\pm}_{y,i}\right|;\qquad V^{*\pm}_{P,i}=V^{*\pm}_{yP,i}=K^{\pm}_{P,i}\cdot\left(d^{*\pm}_{y,i}-d^{*\pm}_{y,i-1}\right),\ \left|d^{*\pm}\right|>\left|d^{*\pm}_{y,i}\right| \qquad (1a,b)$$

$V^{*}_{yP,i}$ and $d^{*}_{y,i}$ being the force and displacement at the i-th yielding point, with the elastic stiffness as function of the gradient of the i-th linear segment and damage index ($0\le\Psi\le1$):

$$K^{\pm}_{P,i}=\left(1-\Psi^{\pm}\right)\cdot K^{\pm}_{i} \qquad (2)$$

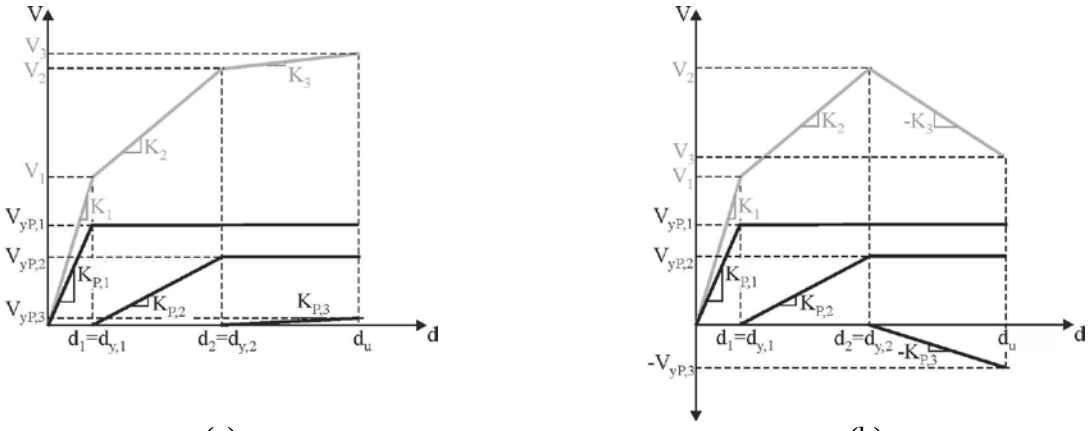

(a) (b)

Fig. 4 – Elastic perfectly-plastic (EPP) mechanisms for hardening (a) and softening (b) branches

Afterwards, the cyclic deterioration is obtained by overlapping damage mechanisms onto the plastic ones (Figs. 5a,b), where the i-th elastic-softening damage (ESD) law is characterized by a first linear upward branch until the attainment of yield displacement of the corresponding i-th plastic mechanism and a second linear downward branch oriented towards the ultimate displacement

$$V^{*\pm}_{D,i}=K^{\pm}_{D,i}\cdot\left(d^{*\pm}-d^{*\pm}_{y,i-1}\right),\ \left|d^{*\pm}_{y,i-1}\right|<\left|d^{*\pm}\right|\le\left|d^{*\pm}_{y,i}\right|;\quad V^{*\pm}_{D,i}=V^{*\pm}_{yD,i}-\frac{d^{*\pm}_{y,i}-d^{*\pm}_{y,i-1}}{d^{*\pm}_{u}-d^{*\pm}_{y,i}}\cdot K^{\pm}_{D,i}\cdot\left(d^{*\pm}-d^{*\pm}_{y,i}\right),\ \left|d^{*\pm}_{y,i}\right|<\left|d^{*\pm}\right|\le\left|d^{*\pm}_{u}\right| \qquad (3a,b)$$

$V^{*}_{yD,i}$ and d^{*}_{u} being the force at the i-th yielding point and the ultimate displacement, respectively, while the elastic and softening stiffnesses are evaluated with following expressions:

$$K^{\pm}_{D,i}=\Psi^{\pm}\cdot K^{\pm}_{i};\quad K^{\pm}_{sD,i}=\frac{d^{*\pm}_{y,i}-d^{*\pm}_{y,i-1}}{d^{*\pm}_{u}-d^{*\pm}_{y,i}}\cdot K^{\pm}_{D,i}=\alpha^{\pm}_{i}\cdot K^{\pm}_{D,i} \qquad (4a,b)$$

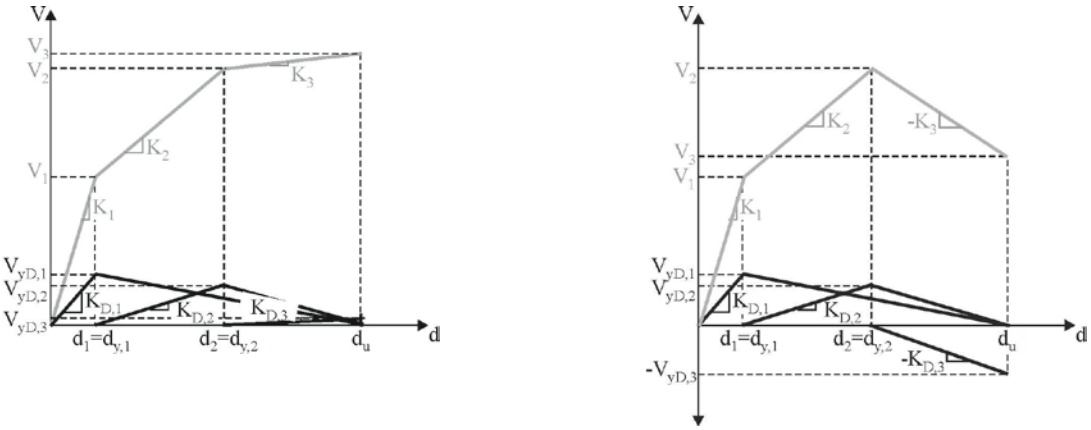

(a) (b)

Fig. 5 – Elastic-softening damage (ESD) mechanisms for hardening (a) and softening (b) branches

Finally, the unloading stiffnesses of the i-th EPP and ESD mechanisms are assumed equal to:

$$K^{\pm}_{uP,i}=\left(1-\Psi^{\pm}\right)\cdot K^{\pm}_{i}=K^{\pm}_{P,i};\quad K^{\pm}_{uD,i}=\alpha^{\pm}_{i}\cdot\frac{d^{*\pm}_{u}-d'^{*\pm}_{i}}{d'^{*\pm}_{i}}\cdot\Psi^{\pm}\cdot K^{\pm}_{i}=\beta^{\pm}_{i}\cdot\Psi^{\pm}\cdot K^{\pm}_{i} \qquad (5a,b)$$

where d' is the displacement of the softening branch corresponding to the initial point of the unloading phase. In this way, the unloading branch of the i-th ESD mechanism is oriented towards the origin.

In order to illustrate how the previous seismic damage of the BF, IF and PF structures influences the DBD procedure of the HYDBs installed along the X and Y directions, piecewise linear approximation of the pushover curves for the equivalent SDOF systems without damage (Ψ=0) are first plotted in Fig. 6. Note that six parameters are involved in the trilinear backbone curves including hardening (Figs. 6b,d,e,f) and softening (Figs. 6a,c) branches. Thus, three pairs of EPP and ESD mechanisms are evaluated for each original structure, where parameters of the i-th pair (i.e. α_i and β_i represented by the Eqs. (4b) and (5b), respectively) are expressed in terms of the displacements defining the characteristic points of the trilinear backbone curve. Nonlinear dynamic analyses of the SDOF systems subjected to the artificial accelerogram above described are carried out, considering low (i.e. Ψ=0.33), medium (i.e. Ψ=0.5) and high (i.e. Ψ=0.83) levels of damage. Finally, the envelope backbone curves are plotted in Fig. 6, considering those with the lowest base shear among negative and positive values. As can be observed, the first (elastic) branch of the cyclic envelopes matches that of the initial backbone curves, while a significant decrease in strength and stiffness occurs for increasing values of the damage index Ψ with a third branch with marked softening.

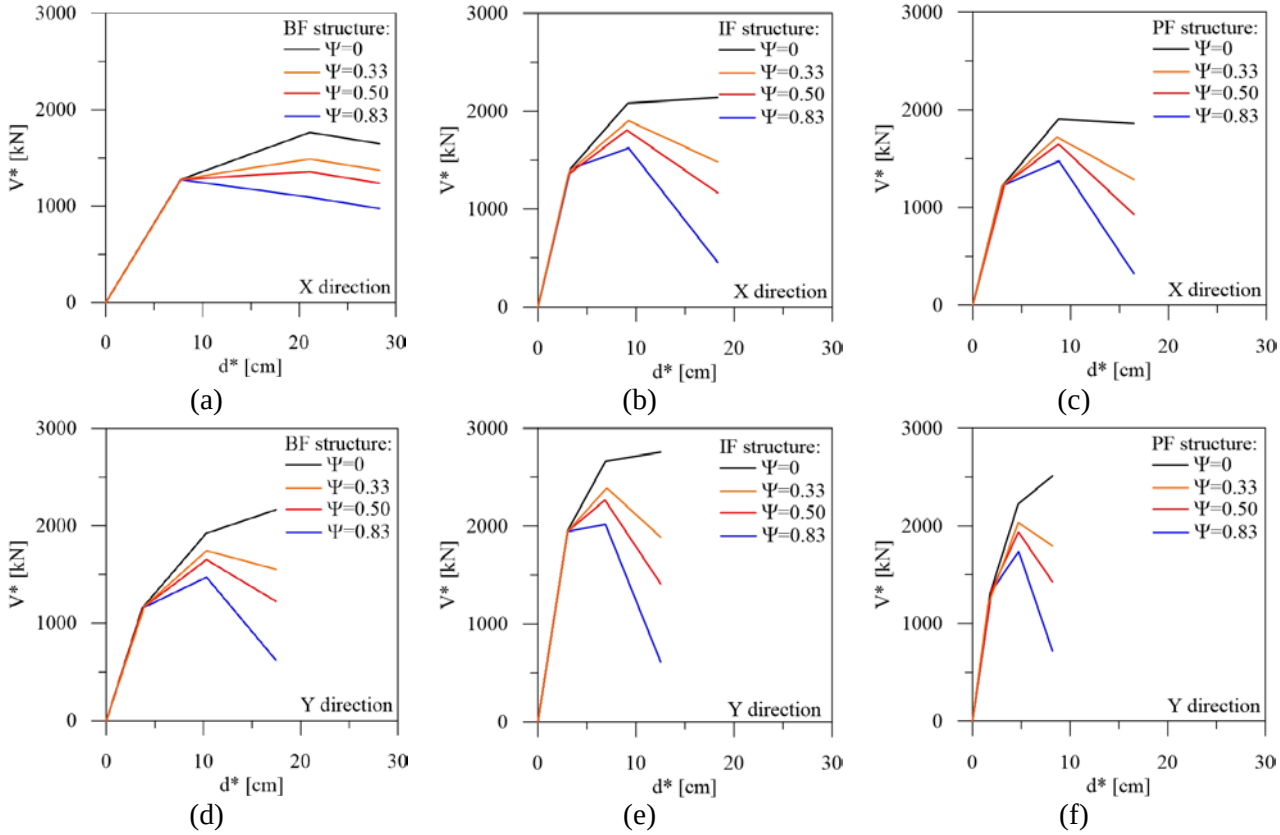

Fig. 6 – Comparison of pushover curves for different levels of damage of the equivalent SDOF system

Finally, an iterative DBD procedure [3, 4, 11] is used to proportion the equivalent HYDBs of the DBBF, DBIF and DBPF structures with reference to Ψ=0 and Ψ=0.5 only. In particular, a variable design value of the frame ductility (i.e. μ_F=1.3-1.8), consistent with the constant performance displacement d_p=9.32 cm, is combined with a constant design value of the damper ductility (i.e. μ_D=5); constant hardening ratios r_F=1% and r_D=3% are also assumed. Values of equivalent stiffness ($K_{DB,e}$) and shear forces at the yielding ($V_{yDB,e}$) and performance ($V_{pDB,e}$) points are reported in Tables 2a-2c. As expected, stiffness and strength properties of the equivalent HYDB are generally greater in the (weakest) X direction rather than in the Y, and for the (brittle) PF structure rather than BF and IF ones. Moreover, note that a significant increase of the equivalent properties is observed when Ψ=0.5 instead of Ψ=0 is assumed, thereby confirming the importance of accounting for the previous nonlinear cyclic response accurately.

Table 2a – Stiffness and strength properties of the equivalent damped brace for DBBF (unit in kN and m)

Direction	$K_{DB,e}$ (Ψ=0)	$V_{yDB,e}$ (Ψ=0)	$V_{pDB,e}$ (Ψ=0)	$K_{DB,e}$ (Ψ=0.5)	$V_{yDB,e}$ (Ψ=0.5)	$V_{pDB,e}$ (Ψ=0.5)
X	4205	391	438	7612	598	669
Y	8161	566	634	25610	1172	1313

Table 2b – Stiffness and strength properties of the equivalent damped brace for DBIF (unit in kN and m)

Direction	$K_{DB,e}$ (Ψ=0)	$V_{yDB,e}$ (Ψ=0)	$V_{pDB,e}$ (Ψ=0)	$K_{DB,e}$ (Ψ=0.5)	$V_{yDB,e}$ (Ψ=0.5)	$V_{pDB,e}$ (Ψ=0.5)
X	9464	590	661	24234	1132	1268
Y	5334	325	364	17034	834	934

Table 2c – Stiffness and strength properties of the equivalent damped brace for DBPF (unit in kN and m)

Direction	$K_{DB,e}$ (Ψ=0)	$V_{yDB,e}$ (Ψ=0)	$V_{pDB,e}$ (Ψ=0)	$K_{DB,e}$ (Ψ=0.5)	$V_{yDB,e}$ (Ψ=0.5)	$V_{pDB,e}$ (Ψ=0.5)
X	11019	635	711	24926	1107	1240
Y	8274	456	510	33481	1241	1390

4. Numerical results

A three-dimensional model for nonlinear dynamic analysis of the original (i.e. BF, IF and PF) and retrofitted (i.e. DBBF, DBIF and DBPF) structures is created in the OpenSees platform [7], taking into account the onset of shear failure in r.c. frame members and joints, prior to or following ductile ones, and the nonlinear in-plane behaviour of masonry infills considered as structural elements [6]. Specifically, the failure mode of beams and columns is predetermined, by classifying each of them as brittle or ductile. Moreover, the HYDBs are simulated with truss elements through a bilinear axial stress-strain law, where yielding and buckling of the diagonal steel braces are assumed to be prevented. Then, seven earthquakes, reflecting the DM18 provisions at the site in question [14], are selected from the Pacific Earthquake Engineering Research Center database [16] and scaled in order to match on average the LS design response spectrum, within lower (i.e. -10%) and upper (i.e. +30%) bound tolerances, in a suitable range of vibration periods. The results are a mean of the maximum values obtained for each of the seven pairs of accelerograms at the final instant of simulation, even if failure modes of structural and non-structural elements generally occur earlier.

First, mean damage index of the rotational springs, lumped at the critical end sections of r.c. elements (i.e. $\Psi_{\theta,e}=\theta_{max,e}/\theta_{u,e}$) and in the joints (i.e. $\Psi_{\theta,j}=\theta_{max,j}/\theta_{u,j}$), and truss elements, representing masonry infills (i.e. $\Psi_{\Delta,i}=\Delta_{max,i}/\Delta_{u,i}$), along the building height is reported in Figure 7. In particular, curves corresponding to the original and retrofitted structures are compared, the latter corresponding to the HYDBs designed with (e.g. Ψ=0.5) and without (i.e. Ψ=0) considering previous seismic damage of the structures. It is interesting to note that a "strong-beam weak-column" mechanism affects the original structures at the lowest two storeys (Figs. 7a-7f), especially for the PF structure where an open ground storey is considered (Figs. 7c,7f), leading to a significant decrease in the global ductility. Moreover, the shear demand in the beam-column joint panels, identified as the main cause of collapse of many buildings during recent earthquakes, is dominant at the third and fourth levels of all existing structures (Figs. 7g-7i). From the second to the fourth level, masonry infills exhibit a medium-high level of the in-plane damage, while little damage is noted at the first and top levels (Figs. 7j,k). Further results, omitted for the sake of brevity, have shown that the maximum damage index related to an earthquake may exceed the corresponding ultimate value, inducing shear failure of columns (i.e. $\Psi_{\theta,e}=1$) and joints (i.e. $\Psi_{\theta,j}=1$) of the staircase along the Y direction, for all the original structures, and brittle failure of masonry infills (i.e. $\Psi_{\Delta,i}=1$), for the IF and PF structures.

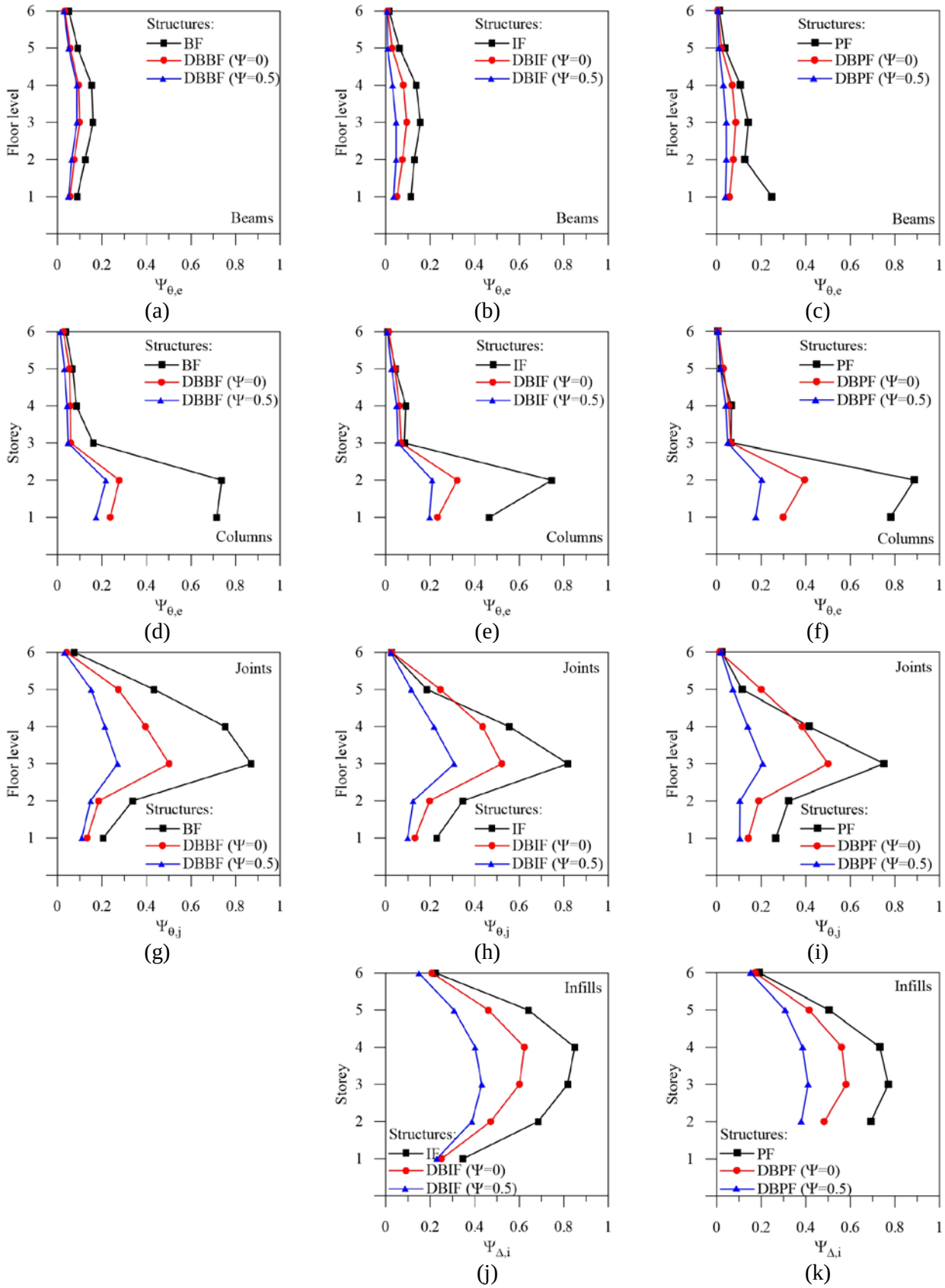

Fig. 7 – Ductile and brittle damage indexes for the original and retrofitted structures

For all the examined case studies, the insertion of the HYDBs represents an effective technique for upgrading capacity, ensuring a notable reduction of the seismic demand of both ductile and brittle failure modes, with an ever greater effectiveness for Ψ=0.5 rather than Ψ=0. Moreover, the probability of collapse of the HYDBs, due to the attainment of ultimate ductility (i.e. μ_{Du}=20), increases when they are designed without considering previous seismic degradation of r.c. frame members (Ψ=0).

Finally, mean values of the storey drift ratio for each level, defined as drift along the in-plan X (Δ_X) and Y (Δ_Y) directions normalized by the storey height (h), are shown in Figure 8. As can be observed, the original structures exhibit higher deformability in the X (Figs. 8a,b,c) rather than in the Y (Figs. 8d,e,f) direction. An irregular distribution law of the drift ratio can be observed for the BF and IF structures, although the NTC18 criteria for regularity in elevation are satisfied. The proportional stiffness criterion, used for the HYDBs of DBBF (Figs. 8a,d) and DBIF (Figs. 8b,e), ensures a reduction of at least half of the drift demand when Ψ=0.5 is assumed, but its distribution is still quite irregular. On the other hand, the constant drift criterion adopted for the DBPF structure improves the shape (almost uniform) and intensity of the drift ratio when previous damage is taken into account (Figs. 8c,f).

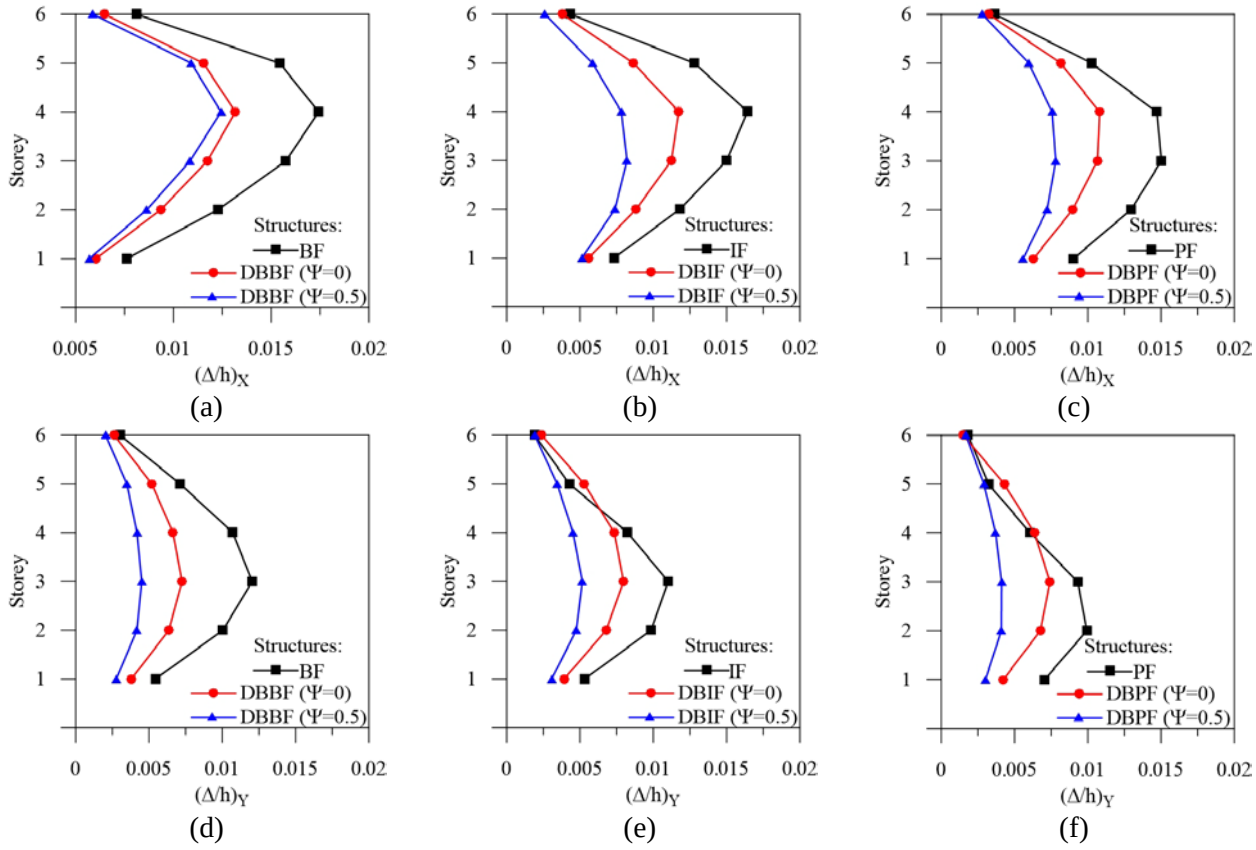

Fig. 8 – Drift ratio for the original and retrofitted structures

5. Conclusions

The study presented focuses on evaluating the influence of previous seismic degradation of r.c. framed buildings retrofitted by hysteretic damped braces. To this end, a displacement-based design procedure of the HYDBs, considering the effects of degrading cyclic response of the r.c. frame members through a simplified plastic-damage hysteretic model, is applied to an archetype representative of the Italian residential buildings built in the 1990s, assuming bare, infilled and pilotis configurations. Based on the results of nonlinear seismic analysis carried out on the OpenSees platform, the following conclusions can be drawn. Brittle failure modes affect the behaviour of the original structures, with a “strong-beam weak-column” mechanism at the lowest two storeys, high shear demand in the beam-column joints and columns of the staircase, at the

third and fourth levels, and medium-high level of the in-plane damage for masonry infills placed from the second to the fourth level. The insertion of the HYDBs ensures a notable reduction of the post-retrofitting seismic demand, with an ever greater effectiveness when previous seismic degradation of r.c. frame members is considered. The irregular distribution law of the drift ratio observed for the original structures is avoided for the DBPF, where the constant drift criterion is used for proportioning the HYDBs along the height, while a reduction of at least half of the drift demand is obtained for Ψ=0.5 also for the DBBF and DBIF where the proportional stiffness criterion is adopted.

6. Acknowledgements

The present work was financed by Re.L.U.I.S. (Italian network of university laboratories of earthquake engineering), in accordance with the Convenzione D.P.C.-Re.L.U.I.S. 2019-2021, WP15, Code Revisions for Isolation and Dissipation.

7. References

[1] Applied Technology Council (2009): Effects of strength and stiffness degradation on seismic response. Technical Report ATC 62/FEMA P440A, Federal Emergency Management Agency, Washington, D.C.

[2] Nuzzo I, Losanno D, Caterino N (2019): Seismic design and retrofit of frame structures with hysteretic dampers: a simplified displacement-based procedure. *Bulletin of Earthquake Engineering*, **17** (5), 2787-2819.

[3] Mazza F, Vulcano A (2015): Displacement-based design procedure of damped braces for the seismic retrofitting of r.c. framed buildings. *Bulletin of Earthquake Engineering*, **13** (7), 2121-2143.

[4] Mazza F, Mazza M, Vulcano A (2015): Displacement-based seismic design of hysteretic damped braces for retrofitting in-elevation irregular r.c. framed structures. *Soil Dynamics and Earthquake Engineering*, **69**, 115-124.

[5] Mazza F (2019): A plastic-damage hysteretic model to reproduce strength stiffness degradation. *Bulletin of Earthquake Engineering*, **17** (7), 3517-3544.

[6] Ricci P, Manfredi V, Noto F, Terrenzi M, De Risi MT, Di Domenico M, Camata G, Franchin P, Masi A, Mollaioli F, Spacone E, Verderame GM (2019): RINTC-E: towards seismic risk assessment of existing residential reinforced concrete buildings in Italy. *COMPDYN 2019, 7th ECCOMAS Thematic Conference on Computational Methods in Structural Dynamics and Earthquake Engineering*, Crete, Greece.

[7] McKenna F, Fenves GL, Scott MH (2000): Open system for earthquake engineering simulation. University of California, Berkeley, CA, 2000.

[8] Ibarra LF, Medina RA, Krawinkler H (2005): Hysteretic models that incorporate strength and stiffness deterioration. *Earthquake Engineering and Structural Dynamics*, **34**(12), 1489-1511.

[9] Alath S, Kunnath SK (1995): Modeling inelastic shear deformation in RC beam-column joints. *Proceedings of the 10th Conference in Engineering Mechanics*, University of Colorado at Boulder, Colorado.

[10] Bertoldi SH, Decanini LD, Gavarini C (1993): Telai tamponati soggetti ad azione sismica, un modello semplificato: confronto sperimentale e numerico. *VI National Conference on Earthquake Engineering, ANIDIS*, Perugia, Italy.

[11] Mazza F (2019): A simplified retrofitting method based on seismic damage of a SDOF system equivalent to a damped braced building. *Engineering Structures*, **200**, 109712, doi: 10.1016/j.engstruct.2019.109712.

[12] DM (1992): Norme tecniche per le opere in c.a. normale e precompresso e per le strutture metalliche. *D.M. 14-02-1992*, Italian Ministry of Public Works, Rome, Italy.

[13] DM (1986): Norme tecniche relative alle costruzioni antisismiche. *D.M. 24-01-1986*, Italian Ministry of Public Works, Rome, Italy.

[14] DM (2018): Norme tecniche per le costruzioni. *D.M. 17-01-2018*, Italian Ministry of the Infrastructures and Transports, Rome, Italy.

[15] Seismoartif (2019): A computer program for generation of artificial accelerograms. https://www.seismosoft.com.

[16] PEER (2014). Pacific Earthquake Engineering Research Center database. https://ngawest2.berkeley.edu.

